Atmos. Chem. Phys., 15, 7003–7015, 2015
www.atmos-chem-phys.net/15/7003/2015/
doi:10.5194/acp-15-7003-2015

Atmospheric Chemistry and Physics
Open Access

Simulation of the isotopic composition of stratospheric water vapour – Part 2: Investigation of HDO / H_2O variations

R. Eichinger[1], **P. Jöckel**[1], **and S. Lossow**[2]

[1]Deutsches Zentrum für Luft- und Raumfahrt e.V. (DLR), Institut für Physik der Atmosphäre, Münchner Straße 20, Oberpfaffenhofen, 82234 Weßling, Germany
[2]Karlsruhe Institute of Technology, Institute for Meteorology and Climate Research, Hermann-von Helmholtz-Platz 1, 76344 Leopoldshafen, Germany

Correspondence to: R. Eichinger (roland.eichinger@dlr.de)

Received: 22 September 2014 – Published in Atmos. Chem. Phys. Discuss.: 28 November 2014
Revised: 24 April 2015 – Accepted: 03 June 2015 – Published: 29 June 2015

Abstract. Studying the isotopic composition of water vapour in the lower stratosphere can reveal the driving mechanisms of changes in the stratospheric water vapour budget and therefore help to explain the trends and variations of stratospheric water vapour during recent decades. We equipped a global chemistry climate model with a description of the water isotopologue HDO, comprising its physical and chemical fractionation effects throughout the hydrological cycle. We use this model to improve our understanding of the processes which determine the patterns in the stratospheric water isotope composition and in the water vapour budget itself. The link between the water vapour budget and its isotopic composition in the tropical stratosphere is presented through their correlation in a simulated 21-year time series. The two quantities depend on the same processes; however, they are influenced with different strengths. A sensitivity experiment shows that fractionation effects during the oxidation of methane have a damping effect on the stratospheric tape recorder signal in the water isotope ratio. Moreover, the chemically produced high water isotope ratios overshadow the tape recorder in the upper stratosphere. Investigating the origin of the boreal-summer signal of isotopically enriched water vapour reveals that in-mixing of old stratospheric air from the extratropics and the intrusion of tropospheric water vapour into the stratosphere complement each other in order to create the stratospheric isotope ratio tape recorder signal. For this, the effect of ice lofting in monsoon systems is shown to play a crucial role. Furthermore, we describe a possible pathway of isotopically enriched water vapour through the tropopause into the tropical stratosphere.

1 Introduction

Variations in stratospheric water vapour alter the radiative heat budget (Forster and Shine, 1999) and the ozone mixing ratios (Shindell, 2001). The processes which control the stratospheric water vapour budget, however, are poorly quantified (Fueglistaler et al., 2009). These processes are temperature-controlled dehydration, convective activity, methane oxidation and isentropic transport.

Due to their physical and chemical properties, water isotopologues have the potential to answer the open questions concerning the origin of stratospheric water vapour. The small mass difference between H_2O and HDO (^{16}O; the hydrogen isotope deuterium D denotes ^2H) leads to different vapour pressures and zero-point energies. This causes equilibrium and kinetic fractionation effects during phase changes and chemical reactions. Each process which controls the stratospheric water vapour budget can be associated with certain fractionation effects and therefore leaves a specific isotopic signature in the water vapour compound (see Moyer et al., 1996; Steinwagner et al., 2010). This isotopic fingerprint allows us to comprehend the history of stratospheric water vapour (Johnson et al., 2001) and, in this way, can assist to explain the trends and variations in its budget.

In addition to in situ and remote-sensing measurements, the comprehensive simulation of the physical and chemical processes of water isotopologues on the global scale is needed to gain an improved understanding of the basic structure of the water isotope ratios in the stratosphere. Model studies of water isotopologues in the upper-troposphere–

lower-stratosphere (UTLS) include approaches from conceptional (Dessler and Sherwood, 2003; Bolot et al., 2013) to one-dimensional (Ridal et al., 2001; Zahn et al., 2006) and two-dimensional (Ridal and Siskind, 2002) models. Schmidt et al. (2005) applied the general circulation model (GCM) GISS-E, in order to study stratospheric entry values of the isotope ratios of water vapour. However, this model has a comparatively low resolution in the stratosphere and accounting for methane oxidation is prescribed with a fixed production rate.

In Part 1 of this article (Eichinger et al., 2015), an extension of the global climate chemistry model (CCM) EMAC (ECHAM MESSy Atmospheric Chemistry; MESSy stands for "Modular Earth Submodel System") was presented and evaluated. This extension, namely the H2OISO (H2O ISOtopologues) submodel, comprises an additional hydrological cycle, including the water isotopologues $H_2^{18}O$ and HDO and their physical fractionation effects, based on previous studies by, e.g., Hoffmann et al. (1998) and Werner et al. (2011). Besides a vertical resolution resolving the tropical tropopause layer (TTL) and simulating the stratospheric dynamics explicitly, this expanded model system also includes the computation of the methane isotopologue CH_3D and its chemical contribution to HDO through oxidation. Results of an EMAC simulation showed good agreement in stratospheric HDO and $\delta D(H_2O)$ with measurements from several satellite instruments:

$$\delta D(H_2O) = \left(\frac{[HDO]/[H_2O]}{R_{VSMOW}} - 1 \right) \cdot 1000. \quad (1)$$

The Vienna Standard Mean Ocean Water (VSMOW; IAEA, 2009) HDO standard is $R_{VSMOW} = 155.76 \times 10^{-6}$ (see Hagemann et al., 1970). Moreover, the results revealed a stratospheric tape recorder which ranges between the pronounced signal of MIPAS (Michelson Interferometer for Passive Atmospheric Sounding) observations (see Steinwagner et al., 2010) and the missing upward propagation of the seasonal signal in the ACE-FTS (Atmospheric Chemistry Experiment Fourier transform spectrometer) retrieval (see Randel et al., 2012).

The results of these simulations are now further analysed, with the aim of identifying the processes which determine the patterns of the isotopic signatures in stratospheric water vapour. The connection between the water vapour budget and its isotope ratio in the tropical stratosphere over the two simulated decades is presented in Sect. 3. The influence of isotope effects during methane oxidation on the $\delta D(H_2O)$ tape recorder signal is investigated in Sect. 4. In Sect. 5 the origin of the Northern Hemisphere (NH) summer signal of the $\delta D(H_2O)$ tape recorder is examined. Its generation exclusively in the NH is shown to be connected with in-mixing of extratropical air and ice lofting in association with clouds in monsoon systems. Furthermore, a possible pathway of isotopically enriched water vapour from the NH troposphere into the tropical stratosphere is presented. These analyses also reveal a possible underestimation of ice overshooting in the applied convection scheme which can have a significant effect on $\delta D(H_2O)$ in the lower stratosphere. This study constitutes the first application of the isotopic composition of water vapour in order to explore the reasons for changes in the stratospheric water vapour budget with global atmosphere chemistry–climate models.

2 Model description and simulation set-up

The MESSy submodel H2OISO, now part of the EMAC model (Jöckel et al., 2005, 2010), comprises an additional hydrological cycle, separate from the actual cycle and including tracers (Jöckel et al., 2008) for the water isotopologues $H_2^{16}O$, HDO and $H_2^{18}O$ in the three phases vapour, liquid and ice, respectively. These tracers are treated identically to the standard state variables for water in the regular hydrological cycle of EMAC, with the addition of the physical fractionation effects for the isotopologues during phase transitions. The representation of these effects follows the water isotopologue-enabled ECHAM (**EC**MWF **Ham**burg) model (see Hoffmann et al., 1998; Werner et al., 2001, 2011). Equilibrium and kinetic fractionation during the evaporation of water from oceans is described by the bulk formula of Hoffmann et al. (1998). Due to the limitations of the applied land surface scheme, we neglect any isotope fractionation from land surfaces (for details, see Werner et al., 2011). The implementation of the cloud and convection parameterisations (CLOUD and CONVECT) in EMAC follows the study of Werner et al. (2011). For condensation within clouds and for the evaporation of cloud water, a closed system is assumed. An open system is used for the deposition of water vapour to ice. Due to the low diffusivities of the isotopologues in the ice phase, no exchange happens between ice and vapour. During the melting of ice and the freezing of water, as well as for the sedimentation of ice, autoconversion, accretion and aggregation, no fractionation is assumed. The representation of the fractionation during the reevaporation of raindrops follows the study by Hoffmann et al. (1998), who assume an isotopical equilibration of 45 % for large drops from convective rain and 95 % for small drops falling from stratiform clouds. Supplementary to this, an explicit accounting function for the contribution of CH_3D oxidation to HDO, including a parameterisation of the deuterium storage in molecular hydrogen, has been developed in order to achieve realistic HDO mixing ratios and $\delta D(H_2O)$ values in the stratosphere. In Part 1 of this article (Eichinger et al., 2015), the model system and the implementation of HDO throughout the hydrological cycle, including its chemical representation, are presented in detail.

An EMAC simulation in the T42L90MA ($\sim 2.8° \times 2.8°$, 90 layers in the vertical up to 80 km (0.01 hPa), explicit middle atmospheric dynamics) resolution was carried out. The simulation was performed with specified dynamics (i.e. "nudged" towards ERA-Interim reanalysis data (ECMWF;

Dee et al., 2011) up to 1 hPa). The "Tiedtke–Nordeng" convection scheme (Tiedtke, 1989; Nordeng, 1994) was applied to the simulation. After starting from steady-state initial conditions in 1982, the simulation was evaluated during the 21 years from 1990 to the end of 2010. A detailed description of the simulation set-up and a description of the applied MESSy submodels are presented in Part 1 of this article (Eichinger et al., 2015). An evaluation of the model's hydrological cycle itself can be found in Hagemann et al. (2006), who assess the EMAC base model ECHAM5. Jöckel et al. (2006) state that the modifications introduced by the MESSy system, as well as by the application of the T42L90MA resolution and nudging, produce a hydrological cycle similar to the results in Hagemann et al. (2006) and consistent with observations. An extensive evaluation of the isotopic composition of water vapour and of its chemical precursor CH_3D in this EMAC simulation in the troposphere and the stratosphere is presented in Part 1 of the article (Eichinger et al., 2015). Overall, a reasonable representation of stratospheric HDO is reached, although with some systematic, but explainable, discrepancies.

3 Time series of H_2O and $\delta D(H_2O)$

Temporal variations in stratospheric water vapour during the last decades have been observed by various instruments. The reasons for these variations are much discussed (see, e.g., Hurst et al., 2011; Dessler et al., 2013; Randel and Jensen, 2013; Hegglin et al., 2014). Before analysing these changes with the EMAC model using the newly implemented HDO, it has to be ensured that the EMAC simulation features the main characteristics of the changes in stratospheric water vapour from 1990 to the end of 2010. Therefore, the equatorial water vapour mixing ratios at 30 km altitude of the simulation are compared with a combined HALOE (HALogen Occultation Experiment) and MIPAS data set in Fig. 1. A detailed description of the combination of the satellite data time series is given in the Supplement. A 2-year running mean was calculated for both time series in order to make the trends more visible by eliminating the signal of the quasi-biennial oscillation (QBO).

The combined HALOE–MIPAS data show an increase in stratospheric water vapour in the first half of the 1990s and a plateau hereafter until the year 2000. The water vapour mixing ratio drops by around 0.3 µmol mol^{-1} between 2000 and 2002 and stays at this lower level until the middle of the first decade of the 21st century. Hereafter, a slow increase can be observed until the end of the time series in 2010. This behaviour of stratospheric water vapour during the previous decades has also been reported and discussed, e.g. by Randel and Jensen (2013), who analysed a combined HALOE and MLS (microwave limb sounder) data set, and is strongly connected to tropopause temperatures.

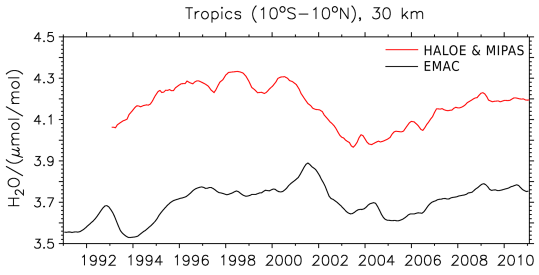

Figure 1. Time series of stratospheric water vapour at 30 km averaged between 10° S and 10° N. Combined HALOE and MIPAS data and the EMAC simulation. Both time series are processed with a 2-year running mean.

The EMAC simulation generally reproduces these variations, although with a constant offset and a few differences. The general dry bias in EMAC has already been discussed by Jöckel et al. (2006) and in Part 1 of this article (Eichinger et al., 2015). Its main reasons are the slightly too cold hygropause in the nudging data (see, e.g., Liu et al., 2010) and the coarse horizontal resolution of the model. In contrast to the satellite observations, in the EMAC simulation the drop around the year 2001 is preceded by an increase in water vapour. Moreover, the level of the water vapour mixing ratio after the drop does not fall below the level of the early 1990s. The Pearson's correlation coefficient between the observed and simulated time series is $R^2 = 0.50$.

In order to estimate the correlation between the changes of water vapour and its isotopic composition, the monthly anomalies with regard to the 21-year monthly averages of the tropical water vapour mixing ratios and $\delta D(H_2O)$ are shown in Fig. 2 for the 21 years of the EMAC simulation at 18 km and at 30 km altitude. Again, the data were processed with a 2-year running mean, in order to obtain a better visibility of the trends. The anomaly of $\delta D(H_2O)$ is divided by 30 for better comparability.

At 18 km altitude, the Pearson's correlation coefficient between the two time series is $R^2 = 0.57$, and this correlation decreases to $R^2 = 0.28$ at 30 km. At 18 km altitude, both quantities are dominated by troposphere–stratosphere exchange processes. At 30 km altitude, the chemical effects, induced by CH_4 oxidation for H_2O and the different lifetimes of CH_4 and CH_3D for $\delta D(H_2O)$, become important. An interdependence of the two quantities can be observed at both altitudes, although, during certain periods, the development of the two time series is anticorrelated. The drop around the year 2001 can be seen in water vapour and in $\delta D(H_2O)$ at both altitudes. At 18 km, the more pronounced feature in $\delta D(H_2O)$, however, is the steep increase before the drop. The amplitude of this increase in $\delta D(H_2O)$ exceeds the amplitude of the drop almost by a factor of 2. Even though most of the variations in the two quantities are in phase, the signs of the anomalies are sometimes inverted. At 18 km altitude, $\delta D(H_2O)$ is generally at a lower level at the end of

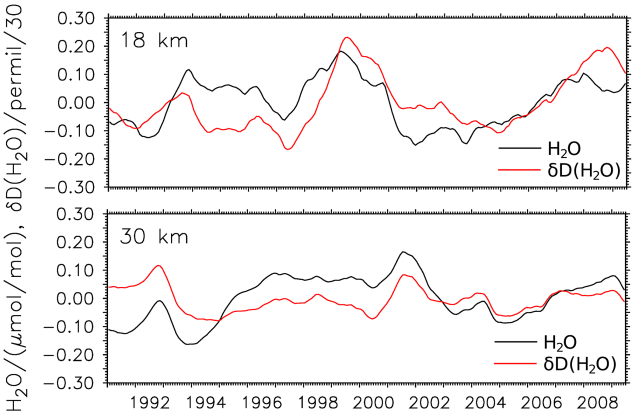

Figure 2. Time series of EMAC-simulated monthly stratospheric water vapour (black) and δD(H_2O) (red) anomalies with regard to the 21-year monthly average at 18 km and at 30 km altitude, averaged between 15° S and 15° N and processed with a 2-year running mean filter. The δD(H_2O) anomalies were divided by 30 for better comparability.

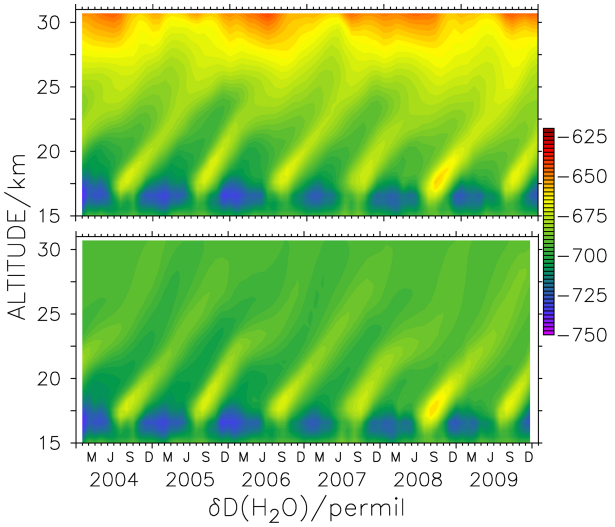

Figure 3. Tropical (15° S–15° N) δD(H_2O) tape recorder signal from 2004 to 2009 in the simulation including (upper panel) and without (lower panel) the effect of methane oxidation on δD(H_2O).

the 1990s compared to the early 2000s, after the drop. The short-term changes, in particular, seem to be different between the two quantities. This suggests that the processes that control stratospheric δD(H_2O) are related but not equal to those that control the stratospheric water vapour budget. The tropopause temperatures, methane oxidation, convective activity and other processes determining water vapour in the stratosphere thus affect stratospheric H_2O and δD(H_2O) with different strengths. Knowledge of this behaviour can therefore help to connect the origin of certain variations and trends to changes in specific processes. The next sections thus aim to reveal the influence of individual processes on stratospheric δD(H_2O), with a special focus on the tape recorder, since the strength of this phenomenon largely determines the intrusion of water vapour into the stratosphere.

4 Sensitivity of the δD(H_2O) tape recorder to methane oxidation

In order to analyse the impact of the contribution of CH_4 and CH_3D oxidation on the δD(H_2O) tape recorder signal, an additional EMAC simulation was conducted. The only difference in this simulation is a modified chemical tendency for HDO. The concept for this sensitivity simulation is an artificial deactivation of the chemical fractionation effects. In other words, δD(H_2O) is not influenced by chemical isotope effects; CH_3D oxidation alters always HDO in relation to CH_4 oxidation, as if there was no isotope fractionation. A detailed description of this modification is given in the Supplement.

For the analysis of the impact of isotope effects during methane oxidation on the δD(H_2O) tape recorder signal, the simulation with the modified HDO tendency is compared to the simulation with regular methane isotope chemistry. The set-up is the same for both simulations. Figure 3 shows the tropical tape recorder signals from 2004 to 2009 for the two simulations from 15 to 30 km.

Between 15 and 25 km, the δD(H_2O) values are similar in both panels. In the tropical tropopause layer and the lower stratosphere, δD(H_2O) is only weakly affected by methane oxidation. From 25 km upwards, increasingly higher δD(H_2O) values can be observed in the simulation with regular methane isotope chemistry (upper panel). The effect of the chemistry on δD(H_2O) increases with altitude in the stratosphere. This can be observed for the increased δD(H_2O) values, which emerge during the NH summer, as well as for the low δD(H_2O) values from the boreal-winter signal. The tape recorder signal in the simulation with the modified methane isotope chemistry (lower panel) extends further up. It is still present, although weak, at the top of this panel at around 30 km altitude. In the upper panel the δD(H_2O) tape recorder signal above 25 km becomes increasingly overshadowed by high δD(H_2O) values, which are generated by the different lifetimes of CH_4 and CH_3D, i.e. chemical isotope effects. The upward-propagating signatures fade out or, more specifically, mix with the high δD(H_2O) values. These high δD(H_2O) values show variations with a phase of around 2 years, which can be associated with the QBO.

For a better quantification of the differences between the two tape recorder signals, Fig. 4 shows the annually averaged difference in the δD(H_2O) maximum and minimum as a function of altitude for the time period of Fig. 3. The black line denotes the simulation with, and the red line the simulation without, the methane effect.

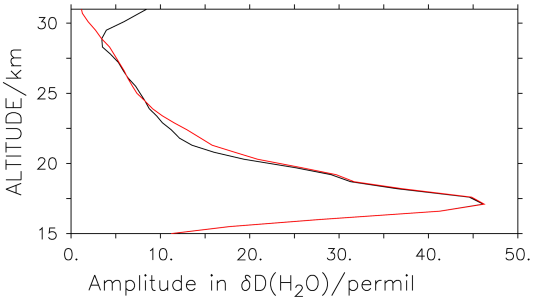

Figure 4. Annually averaged difference between the maximum and the minimum of δD(H_2O) as function of altitude, with (black) and without (red) the effect of methane oxidation on δD(H_2O).

The tape recorder amplitudes are equal below 20 km. As expected, further above, the amplitude of the simulation with chemistry effect on δD(H_2O) decreases more quickly with altitude than the amplitude of the simulation without this effect. The high δD(H_2O) values from the NH summer signal are not affected as strongly by methane oxidation as the low values from the NH winter signal are. To explain this, constant temperatures, and hence fractionation factors, and a constant background δD(CH_4) are assumed, which is reasonable here. The isotope ratios of isotopically different reservoirs show different sensitivities to the addition of a compound with a certain isotope ratio. This means that the smaller the differences between the δ values are, the smaller is the modification. Since the high δD(H_2O) values from the NH summer signal are closer to the δD(CH_4) values (δD(CH_4) is also based on VSMOW), which are around -50 ‰ here, compared to the low δD(H_2O) values from NH winter, the summer signal is altered less. Additionally, the water vapour mixing ratios are also different here. The δD(H_2O) values of the low water vapour mixing ratios from the NH winter signal are therefore again affected more strongly by the addition of (a similar amount of) isotopically enriched water vapour from methane oxidation. This leads to the conclusion that the production of H_2O and HDO by the oxidation of CH_4 and CH_3D reduces the amplitude of the δD(H_2O) tape recorder and overshadows the upward propagation of the signal.

Between 24 and 28 km, the amplitude of the δD(H_2O) variations in the simulation with chemistry effect on δD(H_2O) are similar, and above 28 km the amplitude in the simulation with the chemistry effect exceeds the amplitude of the simulation without. This, however, is not due to the tape recorder effect anymore but is caused by the QBO. The QBO also has an effect on the stratospheric water vapour budget and on the water vapour tape recorder (see Niwano et al., 2003). As stated above, the cycle of the QBO can be seen in the high δD(H_2O) values between 25 and 30 km in Fig. 3. Temperature and hence chemical fractionation factor variations and also dynamical differences between the QBO phases which mix in more or less strongly enriched water vapour lead to this cycle and hence to this increase in amplitude.

5 The origin of the δD(H_2O) tape recorder

Both the water vapour mixing ratio and δD(H_2O) exhibit enhanced values in the lower stratosphere during JJA (June, July, August). The underlying processes for this, however, may differ in some ways for the two quantities. In order to demonstrate this and to analyse the origin of the tape recorder signal, the water vapour mixing ratios and δD(H_2O) in the UTLS for JJA are shown in Fig. 5.

Differences in the distribution of the enhanced values can be observed when comparing the two panels. In the left panel, enhanced H_2O mixing ratios can be seen within almost the entire TTL, although decreasing with altitude and towards the southern latitudes. At the northern edge of the TTL, the high H_2O mixing ratios exceed the tropopause and penetrate into the stratosphere. Some water vapour, however, also intrudes into the stratosphere in the central and the southern TTL. Isotopically enriched water vapour (see right panel) exclusively enters the stratosphere at the northern edge of the TTL. δD(H_2O) values of above -650 ‰ can be observed, crossing the tropopause and entering the tropical pipe here. Note that the enhancement of δD(H_2O) between 17 and 18 km is an artefact caused by the seasonal averaging. The signal originates from the northern edge of the TTL and remains in the tropical pipe during summer while being mixed with surrounding air masses comparatively quickly between 16 and 17 km. In the Supplement, zonal δD(H_2O) across all latitudes is also presented for the other seasons (DJF – December, January, February; SON – September, October, November; MAM – March, April, May) from 10 to 30 km altitude. There, the high δD(H_2O) values in the tropical pipe can still be seen during SON and DJF. In the central and southern parts of the TTL, the water vapour is isotopically strongly depleted, exhibiting values below -700 ‰. Low δD(H_2O) values can be observed down to 14 km altitude in the central and southern TTL, while relatively high water vapour mixing ratios extend up to almost 16 km altitude in this region.

This shows that, in contrast to H_2O, the enhanced isotope ratios in the tropical lower stratosphere during JJA originate exclusively from the NH. However, it is not clear if it originates from the intrusion of tropospheric water vapour into the stratosphere or from in-mixing of old stratospheric air from the extratropics. During DJF a similar signal of isotopically enriched water vapour at the edge of the TTL at around 40° S can be observed (see Supplement). In contrast to the situation in JJA, here this signal is at considerably lower altitudes and does not penetrate into the stratosphere.

In the lower stratosphere, air experiences rapid horizontal transport between the tropics and the midlatitudes above the subtropical jets (Rosenlof et al., 1997). The region be-

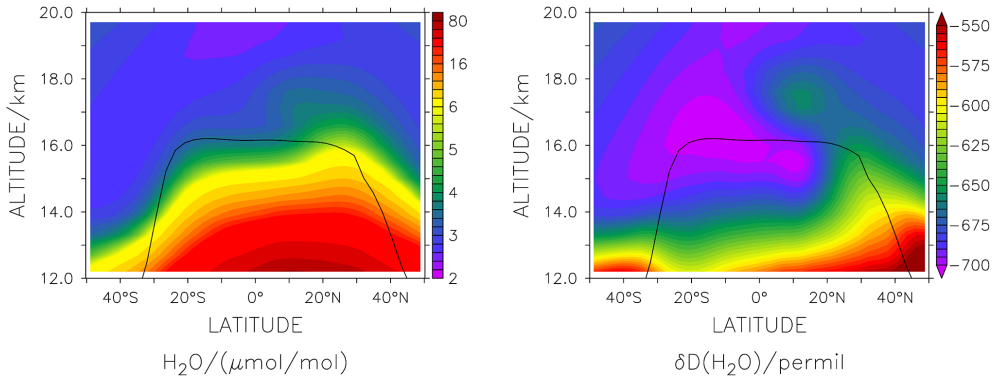

Figure 5. H_2O mixing ratio (left panel) and $\delta D(H_2O)$ (right panel) in the UTLS in JJA averaged over the 21 years of the EMAC simulation. The black lines denote the tropopause.

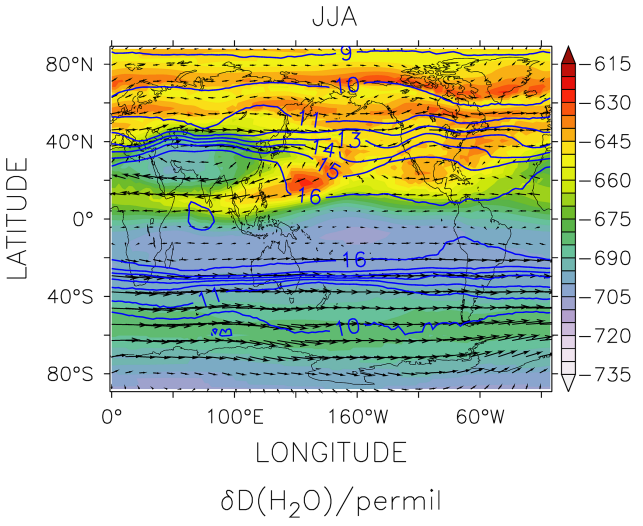

Figure 6. Seasonally averaged $\delta D(H_2O)$ (colours), horizontal wind vectors (arrows) averaged from the 380 to the 400 K isentrope and the tropopause height in kilometres (blue contour lines) in JJA, averaged over the 21 years of the EMAC simulation.

tween the 380 and the 400 K isentrope is therefore crucial for the properties of stratospheric air. To provide an insight into the horizontal dynamics of this region, the average of $\delta D(H_2O)$ between the 380 and the 400 K isentrope is shown in a latitude–longitude representation for JJA in Fig. 6. Again the other seasons are presented in the Supplement.

In general, the image features a pattern with low $\delta D(H_2O)$ in the tropics and increasing values with higher latitudes. In the Northern Hemisphere, patterns can be observed which are associated with the Asian summer monsoon (ASM) and the North American monsoon (NAM). High $\delta D(H_2O)$ values can be seen over the entire North American continent. Over southern Asia, in contrast, very low values are dominant. Around this isotopically depleted centre of the ASM anticyclone, the water vapour is isotopically enriched. Over the West Pacific, at the outflow of the ASM anticyclone, the wind vectors indicate a considerable southward component, which drags isotopically enriched air from the extratropics towards the tropics and then westwards. This air may originate from in-mixing of old stratospheric air from the extratropics. Konopka et al. (2010) show a similar pattern for ozone which, according to Ploeger et al. (2012), can also result in a stratospheric-tape-recorder-like signal. However, Ploeger et al. (2012) state that this process is largely dependent on the species itself, or, more specifically, on its meridional gradient. The study shows that in-mixing plays a role in the annual ozone variations in the tropics but not for carbon monoxide, nitrous oxide or water vapour. Another possible explanation for these patterns is the intrusion of tropospheric air into the stratosphere. Steinwagner et al. (2010) focus especially on slow ascent and dehydration through in situ cirrus formation, which can generate the $\delta D(H_2O)$ tape recorder signal, and Randel et al. (2012) point out the importance of ice overshooting convection on the pattern. In the remainder of this section we will examine some of these mechanisms in order to obtain a better understanding of their relative importance for the $\delta D(H_2O)$ tape recorder.

5.1 In-mixing vs. lofted ice

At first, we will examine whether in-mixing of old stratospheric air from the extratropics alone can suffice to explain the $\delta D(H_2O)$ tape recorder. Water vapour from the extratropical stratosphere has been isotopically enriched through isotope effects during methane oxidation. These effects are relatively even throughout the year and broadly consistent with the chemical production rate of water vapour. A consistent relation between H_2O and $\delta D(H_2O)$ would therefore be expected if in-mixing was the sole factor for this effect. In order to show that this is not the case in the UTLS during JJA, the relation between the water vapour mixing ratios and its isotope ratio is presented in Fig. 7 for JJA and DJF. The black crosses denote this relation in the NH (20 and 40° N)

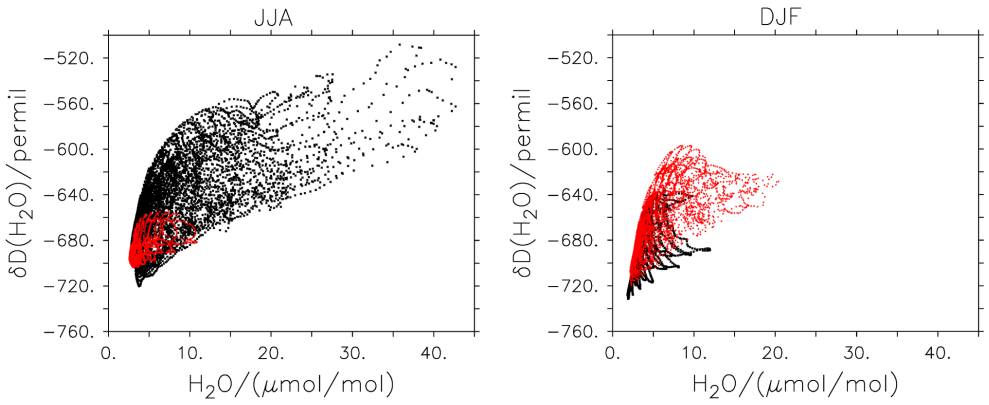

Figure 7. Relation between H_2O and $\delta D(H_2O)$ from 14 to 18 km in JJA (left) and DJF (right) between 20 and 40° N (black crosses) and between 40 and 20° S (red crosses), averaged over the 21 years of the EMAC simulation.

and the red crosses in the Southern Hemisphere (SH) (40 and 20° S), both from 14 to 18 km.

In JJA, the red crosses can be found in a $\delta D(H_2O)$ range between roughly −700 and −660 ‰ with water vapour mixing ratios of up to 10 µmol mol^{-1}. A relationship between increasing $\delta D(H_2O)$ and increasing H_2O mixing ratios is recognisable. The black crosses cover the range of the SH relations as well, but also spread out to higher water vapour mixing ratios and higher $\delta D(H_2O)$ values. Higher water vapour mixing ratios generally feature enhanced $\delta D(H_2O)$ here too, but the black crosses are much more widely distributed, especially for the same water vapour mixing ratios. In DJF, the black crosses cover roughly the range of the red crosses in JJA. The red crosses in DJF, however, hardly spread out to higher H_2O mixing ratios and $\delta D(H_2O)$; thus, the relation differs only slightly between the hemispheres in DJF. The wider distribution of the relation between H_2O and $\delta D(H_2O)$ in the NH during JJA suggests that several processes are important here because a single effect would lead to a rather compact picture in the H_2O to $\delta D(H_2O)$ relation. In particular, this involves the combination of in-mixing of extratropical stratospheric air and the intrusion of tropospheric air into the stratosphere. Crucial tropospheric processes are connected with cloud and convection effects, partly in association with the monsoon systems. As mentioned above, upper-tropospheric water vapour penetrating from the troposphere into the stratosphere could be crucial here. Also, the much discussed influence of ice overshooting convection (see, e.g., Khaykin et al., 2009; Bolot et al., 2013) may have a considerable effect on these patterns.

In order to provide a deeper insight into the ice water content and its isotopic signature, the mixing ratios of ice in the UTLS for JJA (left panel) and DJF (right panel) are shown in Fig. 8. Additionally, $\delta D(ice)$ (the deuterium isotope ratio of the ice water content) is contoured in the figure and the height of the tropopause is marked. The white regions denote ice water mixing ratios below 0.1 µmol mol^{-1}.

The ice water mixing ratios in JJA show two local altitude maxima between roughly 12 and 15 km in this illustration: one in the inner tropics and another one between 30 and 35° N. The latter maximum additionally features high $\delta D(ice)$ at high altitudes up to the tropopause. Ice features δD values of up to −300 ‰ in this area, while the isotope ratio of water vapour lies around −600 ‰ here (see Fig. 5). For DJF, a comparable maximum of lofted ice with high isotopic signatures at these latitudes (in the SH) is not simulated. Lofted ice which resublimates in the upper troposphere could therefore be responsible for the isotopic enrichment of water vapour in this region. The intrusion of this isotopically enriched water vapour into the tropical pipe could then considerably amplify the $\delta D(H_2O)$ tape recorder signal.

5.2 Effects of convective and large-scale clouds

The possible influence of ice lofting into the upper troposphere and an associated isotopic enrichment of the tropical stratosphere during the NH summer will be examined next. For this analysis, we carried out two additional sensitivity simulations with the EMAC model. Analogously to the additional simulation in Sect. 4 with a modified HDO tendency for methane oxidation, we now modified the HDO tendency for large-scale clouds (submodel: CLOUD) and for convection (submodel: CONVECT). These processes control ice lofting and its influence on $\delta D(H_2O)$ in water vapour. Again, the tendency is modified in the manner that $\delta D(H_2O)$ is not altered through the respective process. This enables us to assess the stratospheric $\delta D(H_2O)$ patterns without the influence of either of these two processes and thus to determine their respective contribution on the $\delta D(H_2O)$ tape recorder. Since both of these processes operate almost exclusively in the troposphere, this analysis also allows the separation of the two above-mentioned factors that are thought to control the $\delta D(H_2O)$ tape recorder signal: the in-mixing of old stratospheric water vapour from the extratropics and the intrusion of tropospheric water vapour through the tropopause.

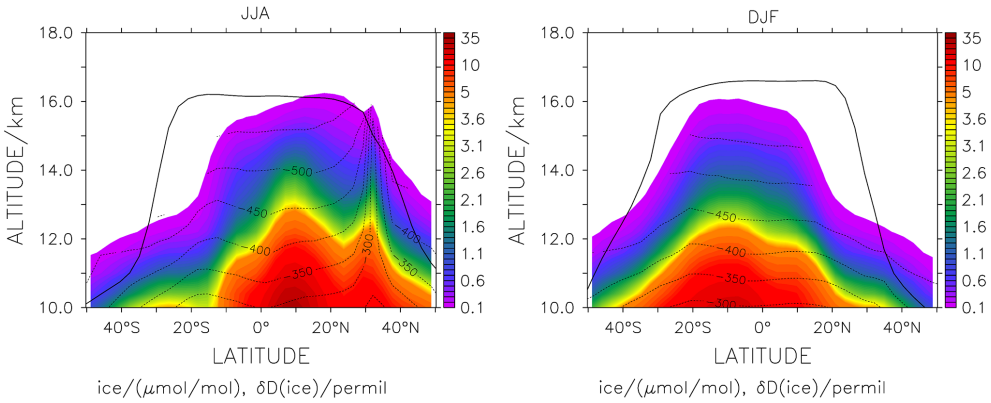

Figure 8. Ice water content (colours) and $\delta D(H_2O)$ in ice (dashed contour lines) in the UTLS in JJA (left) and DJF (right) and tropopause height (solid black line), averaged over the 21 years of the EMAC simulation. The white regions denote ice water mixing ratios below 0.1 µmol mol^{-1}.

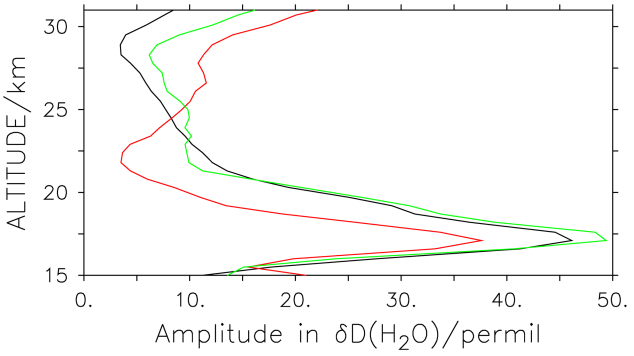

Figure 9. Averaged annual amplitudes of $\delta D(H_2O)$ with altitude, for the standard simulation (black), the simulation without large-scale cloud effect on $\delta D(H_2O)$ (red) and the simulation without the effect of convection on $\delta D(H_2O)$ (green).

Analogously to Fig. 4, the annual amplitudes of $\delta D(H_2O)$ as a function of altitude are shown in Fig. 9. The black line denotes the standard simulation, the red line the simulation with the modified HDO tendency for CLOUD and the green line with the modified HDO tendency for CONVECT.

Around the tropopause, the amplitude of $\delta D(H_2O)$ without the influence of large-scale clouds is smaller and the amplitude without the influence of convection is larger than in the standard simulation. This result is somewhat surprising because, in general, convection is thought to isotopically enrich water vapour, especially during JJA and therefore increase the annual $\delta D(H_2O)$ amplitude. In contrast, the stratosphere is generally isotopically enriched in this simulation compared to the standard simulation, which means that in our model, convection leads to isotopic depletion of the stratosphere. This is likely to be due to the underrepresentation of overshooting convection in the convection scheme applied here. Studies by Dessler et al. (2007) and Bolot et al. (2013) have shown that overshooting convection increases $\delta D(H_2O)$ in the UTLS. By contrast, isotopic depletion through dehydration during the ascent of water vapour seems to dominate in the convection scheme. This process affects HDO more strongly than H_2O and therefore leads to isotopic depletion.

The simulation without the effect of large-scale clouds shows a smaller $\delta D(H_2O)$ amplitude from the tropopause up to around 25 km. In other words, it shows a weaker tape recorder with an earlier fade-out. The stratosphere is generally depleted compared to the standard simulation here, and hence the chemistry affects the pattern more strongly. The smaller $\delta D(H_2O)$ amplitude below 25 km in this simulation shows that the isotopic enrichment during JJA is strongly influenced through large-scale clouds. Hence, ice lofting and the isotopic enrichment of water vapour through resublimation are caused by large-scale clouds in our simulation. A possible mechanism for its influence on the tropical stratosphere will be presented in the following section. In conclusion, the in-mixing of old stratospheric air from the extratropics alone can possibly generate a tape-recorder-like signal for $\delta D(H_2O)$, although strong influences from tropospheric transport induced by large-scale and convective clouds do have a significant impact on the pattern.

5.3 A possible pathway through the tropopause

In order to depict a possible pathway for the isotopically enriched water vapour, which complements the $\delta D(H_2O)$ tape recorder through the effect of ice lofting, the ice water content (left panel) and δD(ice) (right panel) in JJA at 14 km altitude are shown in Fig. 10. The altitude of 14 km was chosen because, as can be seen in Fig. 8, at this altitude the inner tropical and the northern subtropical altitude maxima of the ice water content are still pronounced. This provides information about the source of the influence of ice lofting on the $\delta D(H_2O)$ tape recorder. Regions with ice water mixing ratios below 0.1 µmol mol^{-1} are again shaded white.

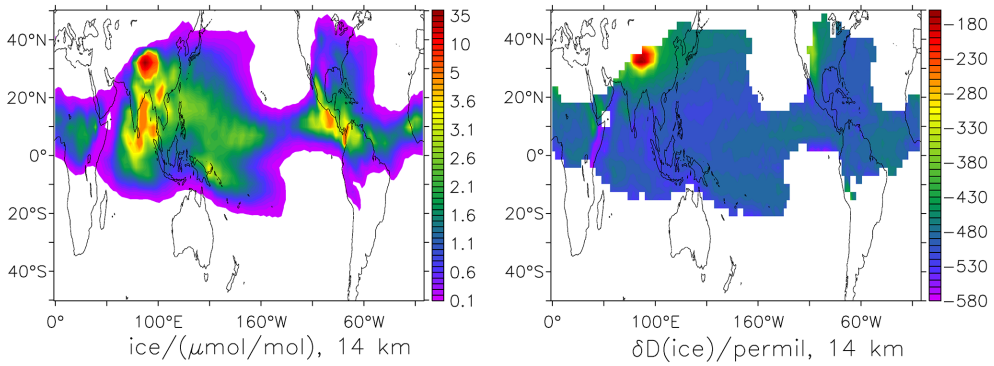

Figure 10. Ice water content (left) and δD(ice) (right) at 14 km altitude in JJA, averaged over the 21 years of the EMAC simulation. The white regions denote ice water mixing ratios below 0.1 µmol mol^{-1}.

The left panel shows several spots of enhanced ice water mixing ratios around the convective zones in the tropics. Especially high ice water mixing ratios can be seen in Southeast Asia and Central America, but by far the highest values are found over the Tibetan Plateau. δD(ice) exhibits a rather uniform picture around the tropics, with values mostly between −500 and −400 ‰. Only one single spot with isotopically enriched ice above the Tibetan Plateau with values above −200 ‰ is noticeably different. This corresponds with the latitude of the altitude maximum in Fig. 8 and suggests that ice lofting over the Tibetan Plateau during the ASM season and associated isotopic enrichment of upper-tropospheric water vapour can possibly account for the major part of this effect. The westerly wind regime in these latitudes (see Fig. 6) can transport the isotopically enriched water vapour from the continent over the West Pacific, where it can enter the stratosphere in the outflow of the ASM anticyclone. Here the tropopause is especially low and crossed by isentropic surfaces. The zonal cross section of δD(H_2O), averaged from 30 to 40° N and presented in Fig. 11, can provide additional evidence for this possible mechanism. Additionally, the tropopause and the isentropes are shown in the figure.

Here, the highest tropospheric δD(H_2O) values can be found at around 100° E, i.e. above the Tibetan Plateau and corresponding with the ASM. Another, weaker maximum lies at around 100° W, which is the location of the Mexican High Plateau and the NAM. A third, even weaker maximum at 0° E can be associated with the North African monsoon. The lowest values are found where the tropopause is highest, i.e. at around 16 km altitude at 50° E. This is also where the temperatures are lowest (not shown). The tropopause height exhibits two minima: one around 160° W and one around 10° W. Around these minima, the highest stratospheric δD(H_2O) values are simulated. The underlying westerly wind regime (shown in Fig. 6) and the tropopause-crossing isentropes in the subtropics thus support the suggestion of an ice lofting effect in association with the monsoon systems contributing to the δD(H_2O) tape recorder.

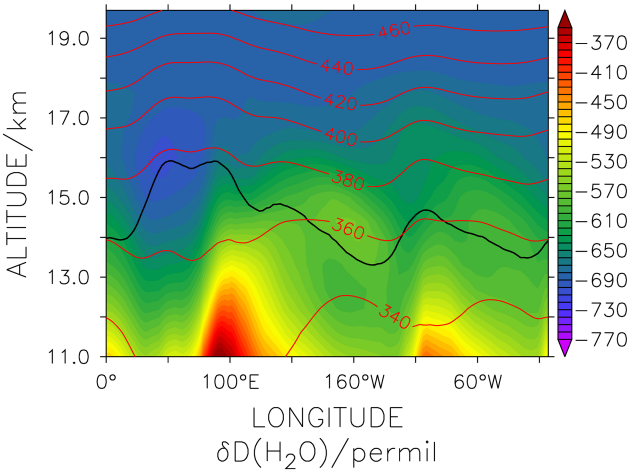

Figure 11. Zonal cross section of δD(H_2O), averaged from 30° N to 40°N for JJA (averaged over the 21 years of the EMAC simulation). The black line denotes the tropopause height; the red contour lines indicate levels of constant potential temperatures (isentropes) in kelvin.

6 Summary and discussion

As a first application of the new H2OISO submodel within the EMAC model, stratospheric water vapour isotope ratios were investigated. The time series of water vapour in the nudged EMAC simulation analysed here reproduces the major variations in the recent decades. The time series of δD(H_2O) shows similarities with H_2O but differs mainly regarding short-term changes. This suggests that the processes controlling these two quantities coincide, but their effect on the respective value is of different quantity.

The impact of methane oxidation on the stratospheric δD(H_2O) tape recorder signal was investigated by comparing the evaluated EMAC simulation with an additional simulation with a suppressed chemical isotope effect of methane oxidation on δD(H_2O). Methane oxidation mainly affects water vapour and its isotopic signature above 25 km, where the

$\delta D(H_2O)$ tape recorder signal fades out faster through this chemical effect. Additionally, the amplitude of the $\delta D(H_2O)$ tape recorder is reduced because methane oxidation influences the low $\delta D(H_2O)$ values and the low water vapour mixing ratios much more strongly than the higher ones. This result is not surprising, but it reveals the impact of the isotope chemistry on the tape recorder. Randel et al. (2012) also applied a correction for the methane effect on $\delta D(H_2O)$ to the ACE-FTS satellite retrieval. This led to the removal of the increase in $\delta D(H_2O)$ with altitude in the stratosphere as well. Moreover, it generated enhanced isotope ratios in the lower stratosphere during JJA and SON, compared to the simulation without the methane correction. However, the $\delta D(H_2O)$ tape recorder is still not clearly visible in the ACE-FTS satellite retrieval.

The determining processes for the generation of enhanced $\delta D(H_2O)$ during JJA in the tropical lower stratosphere were shown to take place exclusively in the NH. This is in contrast to water vapour itself, which is also influenced by direct transport through the TTL (see, e.g., Fueglistaler et al., 2004, 2009). Ploeger et al. (2012) showed that for some species a tape-recorder-like signal can be generated through the in-mixing of old stratospheric air alone. However, Steinwagner et al. (2010) and Randel et al. (2012), for example, focus mostly on the slow ascent of tropospheric water vapour and convective ice overshooting when evaluating the reasons for the generation of the $\delta D(H_2O)$ tape recorder. In order to investigate the role of the individual processes, we first assessed the H_2O to $\delta D(H_2O)$ ratio in the different hemispheres and seasons. A relationship between H_2O and $\delta D(H_2O)$ that is much more spread out during JJA in the NH (compared to the SH and to DJF) suggested that both the intrusion of tropospheric water vapour and the in-mixing of old stratospheric air influence $\delta D(H_2O)$ here. In particular, due to extreme interhemispheric differences in the ice water content and its isotopic signature during the different seasons, the lofting of ice crystals is assumed to enrich water vapour in the NH upper troposphere during JJA. Confirmation is achieved through the results of sensitivity simulations with the modified HDO tendency for large-scale clouds and for convection. The averaged annual difference between the maximum and the minimum of $\delta D(H_2O)$ shows a clear reduction in the UTLS up to 23 km for the simulation without large-scale clouds affecting $\delta D(H_2O)$ and an enhancement for the simulation without convection affecting HDO. The isotopic enrichment during JJA is therefore not generated by convective events, which, in contrast, deplete the water vapour in the simulation, but by large-scale clouds in association with monsoon systems. However, this shows that the $\delta D(H_2O)$ tape recorder is strongly affected by tropospheric effects through clouds and convection and not only by the in-mixing of extratropical air masses.

Augmented ice lofting, especially in the ASM over the Himalayas, has been shown to isotopically strongly enrich the water vapour in the upper troposphere. In the outflow of the monsoonal anticyclones, this isotopically enriched water vapour is transported into the stratosphere on isentropic surfaces. Numerous studies, (e.g. Bannister et al., 2004; Gettelman and Kinnison, 2004; Lelieveld et al., 2007; James et al., 2008) have shown that this sideways transport into the tropics in particular from the ASM also contributes significantly to the stratospheric water vapour budget. By analysing MIPAS satellite data, Steinwagner et al. (2010) suggest that a slow dehydration through cirrus cloud formation plays a key role for the $\delta D(H_2O)$ tape recorder. However, the separation of this particular process within the individual parts of the model, i.e. large-scale and convective clouds, is not easily resolvable. In the model, convective clouds isotopically deplete stratospheric water vapour. However, the relative importance of this individual process for the annual signal has to be further investigated. Randel et al. (2012) present a somewhat different pattern of $\delta D(H_2O)$ in the UTLS by analysing ACE-FTS satellite data. In this retrieval, enriched $\delta D(H_2O)$ at 16.5 km altitude can mostly be found over America, and the patch of high $\delta D(H_2O)$ associated with the ASM, as seen in the EMAC data, is considerably weaker. It is still a matter of debate as to whether convective ice overshooting has a significant effect on the stratospheric water vapour budget (see, e.g., Khaykin et al., 2009). According to Dessler et al. (2007) and Bolot et al. (2013), however, it has a substantial effect on the stratospheric $\delta D(H_2O)$ signature. This ice overshooting occurs mostly in the inner tropics and has the potential to isotopically enrich the tropical lower stratosphere. However, the NAM is also associated with strong convective ice overshooting (see, e.g., Uma et al., 2014). The direct intrusion of ice crystals into the stratosphere is known to be represented rather sparsely by the convection scheme applied here and taken from Tiedtke (1989), and it has been shown to not affect stratospheric $\delta D(H_2O)$ in this simulation. Therefore, this discrepancy between model and observations may be due to the underrepresentation of convective ice overshooting in the applied convection scheme. The NAM region as well as the inner tropics could show considerably higher $\delta D(ice)$ values in the UTLS. Furthermore, this is possibly also the cause for the too low $\delta D(H_2O)$ values in the lower tropical stratosphere in EMAC compared to satellite observations during NH summer, as shown in Part 1 of this article (Eichinger et al., 2015). A more detailed evaluation of this effect can be conducted through the implementation of water isotopologues into other convection schemes of EMAC. Future sensitivity studies can then also resolve the robustness of the patterns discovered here and possibly explain the differences between model results and observations more precisely.

7 Conclusions

The temporal variations in stratospheric $\delta D(H_2O)$ reveal connections to those in water vapour, but they show differences regarding the amplitudes. This provides additional informa-

tion about the underlying processes of the changes and therefore can help to gain a better understanding of the reasons for the trends and variations in the stratospheric water vapour budget. First, however, this requires an understanding and quantification of the influence of the individual processes that are responsible for the patterns of $\delta D(H_2O)$ in the stratosphere. Isotope fractionation effects during methane oxidation blur the $\delta D(H_2O)$ tape recorder signal by damping its amplitude and overshadowing it at higher altitudes. This explains the weaker tape recorder signal in $\delta D(H_2O)$ compared to those in H_2O and HDO. The in-mixing of old stratospheric water vapour with high isotope ratios from the extratropics alone does not suffice to describe the $\delta D(H_2O)$ tape recorder. Instead, the influence of the intrusion of tropospheric water vapour through clouds and convection contribute significantly to this pattern. The isotopic enrichment of upper-tropospheric water vapour through ice lofting in association with monsoon systems and further transport of these air masses into the tropical stratosphere in the outflow account for this influence. However, a quantification of the contributions of the respective processes and also of the individual monsoon systems is yet to be established and first requires further analyses of the discrepancies between the model results and satellite retrievals. These discrepancies indicate possible insufficiencies in the model, i.e. the underrepresentation of overshooting convection. This study has laid the foundations for further analyses in order to determine the connection between the patterns and changes in stratospheric H_2O and $\delta D(H_2O)$. The additional information provided by the water isotope ratio is of significant support in unravelling the factors which contribute to trends and variations in the stratospheric water vapour budget.

Acknowledgements. The authors thank the DFG (Deutsche Forschungsgemeinschaft) for funding the research group SHARP (Stratospheric Change and its Role for Climate Prediction, DFG Research Unit 1095); the study presented here was conducted as part of R. Eichingers PhD thesis under grant number BR 1559/5-1. We acknowledge support from the Leibnitz Supercomputing Center (LRZ), the German Climate Computing Center (DKRZ) and thank all MESSy developers and submodel maintainers for their support. Moreover, we thank H. Garny for an important suggestion and S. Brinkop for important comments on the manuscript. Last but not least, we acknowledge the constructive comments of two anonymous referees, who helped to significantly improve this manuscript.

The article processing charges for this open-access publication were covered by a Research Centre of the Helmholtz Association.

Edited by: P. Haynes

References

Bannister, R. N., O'Neill, A., Gregory, A. R., and Nissen, K. M.: The role of the south-east Asian monsoon and other seasonal features in creating the "tape-recorder" signal in the Unified Model, Q. J. Roy. Meteorol. Soc., 130, 1531–1554, 2004.

Bolot, M., Legras, B., and Moyer, E. J.: Modelling and interpreting the isotopic composition of water vapour in convective updrafts, Atmos. Chem. Phys., 13, 7903–7935, doi:10.5194/acp-13-7903-2013, 2013.

Dee, D. P., Uppala, S. M., Simmons, A. J., Berrisford, P., Poli, P., Kobayashi, S., Andrae, U., M. A. Balmaseda, M. A., Balsamo, G., Bauer, P., Bechtold, P., Beljaars, A. C. M., van de Berg, L., Bidlot, J., Bormann, N. B., Delsol, C., Dragani, R., Fuentes, M., Geer, A. J., Haimberger, L., Healy, S. B., Hersbach, H., Hólm, E. V., Isaksen, L., Kållberg, P., Köhler, M., Matricardi, M., McNally, A. P., Monge-Sanz, B. M., Morcrette, J.-J., Park, B.-K., Peubey, C., de Rosnay, P., Tavolato, C., Thépaut, J.-N., and Vitart, F.: The ERA-Interim reanalysis: configuration and performance of the data assimilation system, Q. J. Roy. Meteorol. Soc., 656, 553–597, 2011.

Dessler, A. E. and Sherwood, S. C.: A model of HDO in the tropical tropopause layer, Atmos. Chem. Phys., 3, 2173–2181, doi:10.5194/acp-3-2173-2003, 2003.

Dessler, A. E., Schoeberl, M. R., Wang, T., Davis, S. M., and Rosenlof, K. H.: Stratospheric water vapor feedback, Proc. Natl. Acad. Sci., 110, 18087–18091, 2013.

Dessler, A. E., Hanisco, T. F., and Füglistaler, S.: Effects of convective ice lofting on H2O and HDO in the tropical tropopause layer, J. Geophys. Res.-Atmos., 112, D18309, doi:10.1029/2007JD008609, 2007.

Eichinger, R., Jöckel, P., Brinkop, S., Werner, M., and Lossow, S.: Simulation of the isotopic composition of stratospheric water vapour – Part 1: Description and evaluation of the EMAC model, Atmos. Chem. Phys., 15, 5537–5555, doi:10.5194/acp-15-5537-2015, 2015..

Forster, P. M. d. F. and Shine, K. P.: Stratospheric water vapour changes as a possible contributor to observed stratospheric cooling, J. Geophys. Res., 26, 3309–3312, 1999.

Fueglistaler, S., Wernli, H., and Peter, T.: Tropical troposphere-to-stratosphere transport inferred from trajectory calculations, J. Geophys. Res., 109, D03108, doi:10.1029/2003JD004069, 2004.

Fueglistaler, S., Dessler, A. E., Dunkerton, J. T., Folkins, I., Fu, Q., and Mote, P. W.: Tropical Tropopause Layer, Rev. Geophys., 47, RG1004, doi:10.1029/2008RG000267, 2009.

Gettelman, A. and Kinnison, D. E.: Impact of monsoon circulations on the upper troposphere and lower stratosphere, J. Geophys. Res., 109, D22101, doi:10.1029/2004JD004878, 2004.

Hagemann, R., Nief, G., and Roth, E.: Absolute isotopic scale for deuterium analysis of natural waters. Absolute D/H ratio for SMOW, Tellus, 22, 712–715, 1970.

Hagemann, S., Arpe, K., and Roeckner, E.: Evaluation of the Hydrological Cycle in the ECHAM5 Model, J. Climate, 19, 3810–3827, 2006.

Hegglin, M. I., Plummer, D. A., Shepherd, T. G., Scinocca, J. F., Anderson, J., Froidevaux, L., Funke, B., Hurst, D., Rozanov, A., Urban, J., von Clarmann, T., Walker, K. A., Wang, H. J., Tegtmeier, S., and Weigel, K.: Vertical structure of stratospheric water vapour trends derived from merged satellite data, Nat. Geosci., 7, 768–776, doi:10.1038/ngeo2236, 2014.

Hoffmann, G., Werner, M., and Heimann, M.: Water isotope module of the ECHAM atmospheric general circulation model: A study on timescales from days to several years, J. Geophys. Res.h, 103, 16871–16896, 1998.

Hurst, D. F., Oltmans, S. J., Vömel, H., Rosenlof, K. H., Davis, S. M., Ray, E. A., Hall, E. G., and Jordan, A. F.: Stratospheric water vapor trends over Boulder, Colorado: Analysis of the 30 year Boulder record, J. Geophys. Res., 116, D02306, doi:10.1029/2010JD015065, 2011.

IAEA: Reference Sheet for VSMOW2 and SLAP2 international measurement standards, International Atomic Energy Agency, Vienna, 5 pp., available at: http://curem.iaea.org/catalogue/SI/pdf/VSMOW2_SLAP2.pdf (last access: 13 May 2015), 2009.

James, R., Bonazzola, M., Legras, B., Surbled, K., and Fueglistaler, S.: Water vapor transport and dehydration above convective outflow during Asian monsoon, Geophys. Res. Lett., 35, L20810, doi:10.1029/2008GL035441, 2008.

Jöckel, P., Sander, R., Kerkweg, A., Tost, H., and Lelieveld, J.: Technical Note: The Modular Earth Submodel System (MESSy) – a new approach towards Earth System Modeling, Atmos. Chem. Phys., 5, 433–444, doi:10.5194/acp-5-433-2005, 2005.

Jöckel, P., Tost, H., Pozzer, A., Brühl, C., Buchholz, J., Ganzeveld, L., Hoor, P., Kerkweg, A., Lawrence, M. G., Sander, R., Steil, B., Stiller, G., Tanarhte, M., Taraborrelli, D., van Aardenne, J., and Lelieveld, J.: The atmospheric chemistry general circulation model ECHAM5/MESSy1: consistent simulation of ozone from the surface to the mesosphere, Atmos. Chem. Phys., 6, 5067–5104, doi:10.5194/acp-6-5067-2006, 2006.

Jöckel, P., Kerkweg, A., Buchholz-Dietsch, J., Tost, H., Sander, R., and Pozzer, A.: Technical Note: Coupling of chemical processes with the Modular Earth Submodel System (MESSy) submodel TRACER, Atmos. Chem. Phys., 8, 1677–1687, doi:10.5194/acp-8-1677-2008, 2008.

Jöckel, P., Kerkweg, A., Pozzer, A., Sander, R., Tost, H., Riede, H., Baumgaertner, A., Gromov, S., and Kern, B.: Development cycle 2 of the Modular Earth Submodel System (MESSy2), Geosci. Model Dev., 3, 717–752, doi:10.5194/gmd-3-717-2010, 2010.

Johnson, D. G., Jucks, K. W., Traub, W. A., and Chance, K. V.: Isotopic composition of stratospheric water vapor: Implications for transport, J. Geophys. Res., 106, 12219–12226, 2001.

Khaykin, S., Pommereau, J.-P., Korshunov, L., Yushkov, V., Nielsen, J., Larsen, N., Christensen, T., Garnier, A., Lukyanov, A., and Williams, E.: Hydration of the lower stratosphere by ice crystal geysers over land convective systems, Atmos. Chem. Phys., 9, 2275–2287, doi:10.5194/acp-9-2275-2009, 2009.

Konopka, P., Grooß, J.-U., Günther, G., Ploeger, F., Pommrich, R., Müller, R., and Livesey, N.: Annual cycle of ozone at and above the tropical tropopause: observations versus simulations with the Chemical Lagrangian Model of the Stratosphere (CLaMS), Atmos. Chem. Phys., 10, 121–132, doi:10.5194/acp-10-121-2010, 2010.

Lelieveld, J., Brühl, C., Jöckel, P., Steil, B., Crutzen, P. J., Fischer, H., Giorgetta, M. A., Hoor, P., Lawrence, M. G., Sausen, R., and Tost, H.: Stratospheric dryness: model simulations and satellite observations, Atmos. Chem. Phys., 7, 1313–1332, doi:10.5194/acp-7-1313-2007, 2007.

Liu, Y. S., Fueglistaler, S., and Haynes, P. H.: Advection-condensation paradigm for stratospheric water vapor, J. Geophys. Res., 115, D24307, doi:10.1029/2010JD014352, 2010.

Moyer, E. M., Irion, F. W., Yung, Y. L., and Gunson, M. R.: ATMOS stratospheric deuterated water and implications for troposphere-stratosphere transport, Geophys. Res. Lett., 23, 2385–2388, 1996.

Niwano, M., Yamazaki, K., and Shiotani, M.: Seasonal and QBO variations of ascent rate in the tropical lower stratosphere as inferred from UARS HALOE trace gas data, J. Geophys. Res., 108, D244794, doi:10.1029/2003JD003871, 2003.

Nordeng, T. E.: Extended version of the convection parameterization scheme at ECMWF and their impacts upon the mean climate and transient activity of the model in the tropics, Research Dept. Tech. Memo, 206, European Centre for Medium–Range Weather Forecast, Reading, UK, 41 pp., 1994.

Ploeger, F., Konopka, P., Müller, R., Fuelglistaler, S., Schmidt, T., Manners, J., Grooß, J., Günther, G., Forster, P., and Riese, M.: Horizontal transport affecting trace gas seasonality in the Tropical Tropopause Layer (TTL), J. Geophys. Res., 117, D09303, doi:10.1029/2011JD017267, 2012.

Randel, W. J. and Jensen, E. J.: Physical processes in the tropical tropopause layer and their roles in a changing climate, Nat. Geosci., 6, 169–176, 2013.

Randel, W. J., Moyer, E., Park, M., Jensen, E., Bernath, P., Walker, K., and Boone, C.: Global variations of HDO and HDO/H_2O ratios in the upper troposphere and lower stratosphere derived from ACE-FTS satellite measurments, J. Geophys. Res., 117, D06303, doi:10.1029/2011JD016632, 2012.

Ridal, M. and Siskind, D. E.: A two-dimensional suimulation of the isotopic composition of water vapor and methane in the upper atmosphere, J. Geophys. Res., 107, D24,4807, doi:10.1029/2002JD002215, 2002.

Ridal, M., Jonsson, A., Werner, M., and Murtagh, D. P.: A one-dimensional simulation of the water vapor isotope HDO in the tropical stratosphere, J. Geophys. Res., 106, 32283–32294, 2001.

Rosenlof, K. H., Tuck, A. F., Kelly, K. K., Russel, J. M., and McCormick, M. P.: Hemispheric asymmetries in water vapor and inferences about transport in the lower stratosphere, J. Geophys. Res., 102, 13213–13234, 1997.

Schmidt, G. A., Hoffmann, G., Shindell, D. T., and Hu, Y.: Modeling atmospheric stable water isotopes and the potential for constraining cloud processes and stratosphere-troposphere water exchange, J. Geophys. Res., 110, D21314, doi:10.1029/2005JD005790, 2005.

Shindell, D. T.: Climate and ozone response to increased stratospheric water vapor, Geophys. Res. Lett., 28, 1551–1554, 2001.

Steinwagner, J., Füglistaler, S., Stiller, G., von Clarmann, T., Kiefer, M., Borsboom, P.-P., van Delden, A., and Röckmann, T.: Tropical dehydration processes constrained by the seasonality of stratospheric deuterated water, Nat. Geosci., 3, 262–266, doi:10.1038/NGEO822, 2010.

Tiedtke, M.: A comprehensive mass flux scheme for cumulus parameterization in large-scale models, Mon. Weather Rev., 117, 1779–1800, 1989.

Uma, K. N., Das, S. K., and Das, S. S.: A climatological perspective of water vapor at the UTLS region over different global monsoon regions: observations inferred from the Aura-MLS and reanalysis data, Clim. Dynam., 43, 407–420, doi:10.1007/s00382-014-2085-9, 2014.

Werner, M., Heimann, M., and Hoffmann, G.: Isotopic composition and origin of polar precipitation in present and glacial climate simulations, Tellus B, 53B, 53–71, 2001.

Werner, M., Langebroek, P. M., Carlsen, T., Herold, M., and Lohmann, G.: Stable water isotopes in the ECHAM5 general circulation model: Toward high-resolution isotope modeling on a global scale, J. Geophys. Res., 116, D15109, doi:10.1029/2011JD015681, 2011.

Zahn, A., Franz, P., Bechtel, C., Grooß, J.-U., and Röckmann, T.: Modelling the budget of middle atmospheric water vapour isotopes, Atmos. Chem. Phys., 6, 2073–2090, doi:10.5194/acp-6-2073-2006, 2006.